Applied Physics A (2019) 125:424
https://doi.org/10.1007/s00339-019-2714-6

Applied Physics A
Materials Science & Processing

T.C.: DEDICATED TO MARIA DINESCU

Tuning the physicochemical properties of hernia repair meshes by matrix-assisted pulsed laser evaporation

Cristian Daniel Alin[1,2] · Florin Grama[1,2] · Raluca Papagheorghe[3] · Simona Brajnicov[4] · Valentin Ion[4] · Sorin Vizireanu[4] · Alexandra Palla-Papavlu[4] · Maria Dinescu[4]

Received: 19 March 2019 / Accepted: 15 May 2019 / Published online: 23 May 2019

Abstract

This work was aimed at the fabrication and characterization of hernia repair mesh coatings as innovative solutions that facilitate optimal local integration of implants and prevent the risk of infection. The concept involves the application of a laser-based technique, i.e., matrix-assisted pulsed laser evaporation (MAPLE), for the deposition of polymer/carbon nanotube blends as thin layers on monofilament, macroporous polypropylene, and polyester meshes. Various polymer/carbon nanotube blends are chosen to be deposited as thin layers on the primary blanks (i.e., commercially available meshes). The chosen materials are single-walled carbon nanotubes (CNTs) and poly(ethylene oxide) (PEO) polymer. Carrying out morphological investigation of the as-deposited coatings, i.e., by atomic force microscopy and scanning electron microscopy, we found that the morphology and topography of the PEO/CNT coatings may be tuned by varying the concentration of CNT in the starting material. By increasing the concentration of CNTs in the as-deposited films, they become smoother. In addition, by investigating the chemistry of the coatings surface, we found that it is possible to deposit PEO/CNT coatings by MAPLE with an unaltered chemical structure. In addition, XPS investigation revealed that the films with the 20% CNT are CNT-like, while the films with 2% CNT are PEO-like. The ability to control the morphological and structural properties of the PEO/CNTs blends covering the primary hernia repair meshes demonstrates that MAPLE is a suitable technique for the manufacture of healthcare-intended systems.

1 Introduction

Nowadays, meshes are the most widespread implant materials used in general surgery, i.e., over 20 million implants being used every year in the world [1]. The use of meshes to repair parietal defects is accepted as a general standard, both in classical surgical procedures and in the minimally invasive procedures (laparoscopy), meshes being applied in over 80% of the parietal reconstruction surgeries. Therefore, in the biomedical area, the focus is set on developing both different surgical techniques as well as new materials which allow the integration of the synthetic material in the local anatomy. However, even though the usage of meshes in surgeries is more and more frequent, their optimum integration in the body is still a complex subject, and the risk associated with infections remains one of the main unsolved issues [2].

The market for medical implants offers a wide variety of materials for meshes, i.e., over 70 types of meshes being available today on the market. The most common types of meshes are synthetic, based on polypropylene (PP) and polyester (PE), as they fulfill the requirements for mechanical resistance, optimum biological tolerance, they are chemically inert, and they have stable physical characteristics, flexibility, biocompatibility, etc. [3]. In addition to the physical and chemical properties of the meshes, an important aspect to be considered is bacteria adherence to the meshes and the formation of a biofilm, which leads to increased dosage of antibiotics and finally mesh removal from the body [4]. Therefore, there is a need for new and innovative solutions

✉ Florin Grama
florin_gramma@yahoo.com

✉ Alexandra Palla-Papavlu
alexandra.papavlu@inflpr.ro

[1] General Surgery Department, Colțea Hospital, Bucharest, Romania

[2] "Carol Davila" University of Medicine and Pharmacy, Bucharest, Romania

[3] Central Laboratory, Colțea Hospital, Bucharest, Romania

[4] Lasers Department, National Institute for Lasers, Plasma, and Radiation Physics, Atomiștilor 409, 077125 Măgurele, Romania

to block the infections at the mesh, and new coatings which may stop the formation of biofilms and act to remove and repel bacteria in order to decrease the inflammatory local response [5].

Currently, there is a plethora of studies devoted to the improvement in the physicochemical properties of the meshes. Despite respecting the aseptic measures and using antibioprophylaxis, even in the minimally invasive procedures, the postsurgical infections may reach 3% in the laparoscopic approach and 10% in open surgery. Thus, there is increased interest for new and improved meshes that allow the decrease in postsurgery infections and overcome the need for removal of the meshes in additional surgeries, which in turn increases the cost and the morbidity associated with the procedures [6, 7].

In this work, we are using a laser-based technique to coat conventional, commercially available meshes with polymer/carbon nanotube blends which could eventually be promising solutions for the treatment of hernia repairs. We study the possibility to deposit polymer/carbon nanotube blends on non-conventional, non-planar substrates, i.e., hernia repair meshes, and evaluate the physical and chemical properties of these films. This work is a proof of concept where we show for the first time the deposition of polymer/carbon nanotube blends onto flexible, non-planar substrates.

Here, we apply matrix-assisted pulsed laser evaporation (MAPLE) for the deposition of polyethylene oxide (PEO) and a blend of the PEO and carbon nanotubes (CNT) onto PE and PP meshes. Polyethylene oxide is an amphiphilic, water-soluble synthetic polyether that is available in a range of molecular weights [8, 9]. Commonly, PEOs with $M_w < 100{,}000$ are called polyethylene glycol (PEG). PEO is a nontoxic polymer, and it is used in a wide range of applications, in particular, in the biomedical field, in drug delivery systems, tissue engineering scaffolds, surface functionalization, just to name a few [10].

Furthermore, single-walled carbon nanotubes (SWCNT) have been demonstrated to have a strong toxic effect on bacteria [11, 12]. The physicochemical properties of SWCNT, i.e., chemical stability, thermal conductivity, mechanical strength and ease of functionalization, etc., make them interesting elements to be integrated in biomaterials with antimicrobial properties. Due to the high costs associated with the synthesis and purification of carbon nanotubes, it is unlikely that CNTs alone will be used in healthcare applications. Therefore, it is of great interest to investigate the possibility to fabricate biological coatings based on polymers combined with CNTs as a minority component.

MAPLE is a technique which has been proven for the deposition of polymer films and biomaterials [13, 14], including carbon nanotubes and CNT/polymer composite films [15–17]. MAPLE is derived from the classical pulsed laser deposition (PLD), the difference being the procedure to fabricate the target [13]. In PLD, the laser beam interacts with a target material, solid or liquid, a plume being formed that is transporting the ablated species to a substrate placed parallel, thus a thin film being formed. The disadvantage of PLD for the deposition of polymers, biopolymers, and proteins is that due to the direct interaction of the laser light with the target material, photochemical, or thermal decomposition may occur. Therefore, in MAPLE, the guest material is suspended in a solvent which is named matrix, and the mixture is then flash-frozen in liquid nitrogen, resulting in a solid target. The advantage of MAPLE over PLD for the deposition of organic materials is that the matrix absorbs the laser radiation, and the guest material is collected, similar to PLD, onto a substrate placed parallel to the target. By respecting the two main conditions of MAPLE, i.e., a high absorption of the laser light in the matrix, and as little absorption as possible by the guest material and (2) no photochemical interaction of the matrix with the guest material, a broad range of materials have been deposited, from polymers [18–20], to active proteins such as lactoferrin [21], nanoparticles [22, 23], and polymer/carbon nanotube composites [15, 24]. Recent works are focused on the deposition by MAPLE of PEO as a model semicrystalline polymer with the aim of understanding the differences in the resulting film morphology and thermal properties [25–27]. Moreover, MAPLE has been successfully used to coat sensor devices [28, 29].

2 Experimental

2.1 Materials and substrates

The guest materials are polyethylene oxide (PEO) with an average molecular weight of 100 kDa and single-walled carbon nanotubes (CNT) obtained from Sigma-Aldrich. The individual average diameter of the CNTs is ~ 0.78 nm and the individual CNT length is ~ 1000 nm. For the preparation of the CNT solutions to be used as targets in the matrix-assisted pulsed laser evaporation experiments, the CNTs are dispersed in double-distilled water (which is used as matrix) to 4 wt% solutions in a sonicator for 30 min. Similarly, for the preparation of the PEO solutions to be used as targets in the MAPLE experiments, the PEO polymer is dispersed in double-distilled water (which is used as matrix) to 4 wt% solutions in a sonicator for 30 min. In addition, 4 wt% polymer/carbon nanotube (PEO/CNT) solutions in double-distilled water are prepared. CNT is present either at 2 wt% (hereafter the resulting thin films will be identified as PEO98:CNT2) or 20 wt% (hereafter the resulting thin films will be identified as PEO80:CNT20) in the PEO/CNT solution. In order to improve the dispersion of the carbon nanotubes in the polymer/carbon nanotube mixtures, 2 mg/ml of

sodium dodecyl sulfate has been added to the final solution. The polymer, polymer/carbon nanotube, and carbon nanotube solutions (different experiments) are then flash-frozen in liquid nitrogen resulting in solid targets which are used in the MAPLE experiments.

In this work, two types of substrates are used: (1) double-polished silicon substrates Si(100) cut into 1 cm^2 samples, which are transparent in the IR further and which are used for postcharacterization, and (2) two types of hernia repair meshes: monofilament macroporous polypropylene mesh with low density of 46 g/m^2, and monofilament macroporous polyester low-density mesh (45 g/m^2). The Si(100) substrates are cleaned prior to the MAPLE depositions, by ultrasonication in successive baths of ethanol, followed by rinsing them in the ultrasonic bath with ultrapure water, and drying in a stream of nitrogen.

2.2 Coating of the hernia repair meshes by matrix-assisted pulsed laser evaporation (MAPLE)

The 266 nm laser beam from a "Surelite II" pulsed Nd:YAG laser system (Continuum Company) is imaged on the frozen target (in different experiments, PEO, CNT, and PEO/CNT targets). When the laser light irradiates this target, the solvent evaporates and the guest material is subsequently collected on the substrate. The laser fluence applied for the deposition of the films is set at 750 mJ/cm^2. The substrates are placed at a distance of 3.6 cm from the frozen target.

The substrates are kept at ambient temperature during the deposition. The number of pulses is varied from 12,000 pulses to 126,000, resulting in coatings with variable thicknesses. The target is rotated during the deposition in order to achieve uniform evaporation of the target material.

In order to control the temperature, one thermocouple is placed on a fixed position on the target holder. The background pressure, i.e., 1×10^{-5} mbar, is obtained with a Pfeiffer-Balzers TPU 170 turbomolecular pump (170/Ls). During some depositions, the pressure varied slightly (between 1 and 2×10^{-5} mbar), most probably due to outgassing of the targets under vacuum.

2.3 Surface analysis: Fourier transformed infrared spectroscopy (FTIR), X-ray photoelectron spectroscopy (XPS), and contact-angle measurements

The FTIR measurements are carried out with a Jasco FT/IR-6300 type A spectrometer in the range 600–3200/cm. All spectra are obtained by absorption measurements, accumulating 128 scans, and CO_2/H_2O correction.

XPS survey spectra and high-resolution XPS scan spectra are acquired for the PEO, CNT, and PEO/CNT films deposited by MAPLE using an ESCALAB Xi^+ system, Thermo Scientific. The survey scans are acquired using Al Kα gun, with spot size 900 μm, pass energy of 50.0 eV, energy step size 1.00 eV, and five scans ware accumulated, while for the high-resolution XPS spectra, the pass energy is set to 20.0 eV, and energy step size is 0.10 eV and 10 scans are accumulated. The high-resolution spectra are fitted using Voigt functions (Gaussian–Lorentzian convolutions) and Shirley line-shapes background, using a procedure described previously [30]. The component positions are fixed in accordance with the binding energies (BE) of each sub-peak (component) and its width [full width at half maximum (FWHM)] are kept the same for similar sub-peaks.

Contact-angle measurements are carried out with a KSV CAM101 microscope equipped with a video camera. All contact-angle measurements are obtained by applying the sessile drop method, i.e., a syringe is used which disperses double-distilled water droplets with a volume of 2.5 ± 0.5 μl. Five different points are measured for every thin film, and the contact angle reported is the average of these measurements.

2.4 Morphological investigation: atomic force microscopy (AFM) and scanning electron microscopy (SEM)

Atomic force microscopy (AFM) (XE 100 AFM setup from Park) measurements are carried out to analyze the films thickness as well as surface roughness on several different areas and dimensions (5×5 μm^2). All AFM images are obtained at ambient conditions. Scanning electron microscopy (SEM) is used as a complementary technique to analyze the surface of the MAPLE-deposited films. SEM is carried out on a field emission scanning electron microscope (Inspect S Electron Scanning Microscope, FEI Company) operating at 5 kV.

2.5 Optical measurements: spectroscopic ellipsometry (SE)

The refractive index and extinction coefficient of the polymer and carbon nanotube mixtures deposited as thin films are determined by spectroscopic ellipsometry. Optical measurements are carried out with a Woollam variable-angle spectroscopic ellipsometer (VASE) system, equipped with a high-pressure Xe discharge lamp incorporated in an HS-190 monochromator. Measurements are carried out in the visible and near-UV region of the spectrum, with a step of 2 nm at 60° angle of beam incidence. The calculation of refractive index and extinction coefficients is realized by V-VASE32 software.

3 Results and discussion

3.1 Surface investigation: FTIR, XPS, and contact-angle measurements

The scope of this study is to demonstrate the fabrication of a proof-of-concept system where commercially available hernia repair meshes are coated with thin films by laser-based techniques. Here we focus on investigating the surface chemistry and morphology of the biological coatings fabricated by MAPLE, as the surface of the coatings is susceptible to contamination by bacterial adhesion and biofilm formation [5]. Suppression of biofilm formation is of particular importance in order to avoid mesh infection requiring explantation.

First, we apply Fourier transform infrared spectroscopy (FTIR) to study the characteristic vibrations of the functional groups in the MAPLE-deposited films. The FTIR measurements of PEO and PEO/CNT films are shown in Fig. 1. The acquired spectra of the PEO film deposited at 750 mJ/cm^2 laser fluence, shown in Fig. 1, are similar to those reported for pure PEO in [31]. In the FTIR spectra of MAPLE-deposited PEO, the CH_2 rocking mode may be observed at 841/cm, the CH_2 twisting mode at 1279/cm, the CH_2 wagging mode at 1360 and 1341/cm, the CH_2 scissoring mode at 1466/cm, while the C–H stretching mode can be observed at 2876/cm. The –C–O–C triplet peak, i.e., 1059/cm, 1095/cm, and 1145/cm, with maximum intensity at 1095/cm confirms the semicrystalline phase of PEO [28]. No important changes in the peak positions have been noticed for the pure PEO films deposited by MAPLE, indicating that the polymer has not suffered any structural damages/changes during the MAPLE deposition process. The IR spectra of the PEO/CNT films have no serious modification as compared to the pure PEO spectrum, which could be associated with the absence of interactions between PEO and CNT. However, CNTs are chemically inert materials, and because the van der Waals' attraction causes a significant agglomeration, they do not show noteworthy IR signals [32].

Therefore, in order to gain more information on the surface groups of the MAPLE-deposited PEO, CNT, and PEO/CNT films, XPS analysis is carried out on the same samples. In particular, the physicochemical properties of the thin-film surfaces determine the kinetics of bacteria adhesion. In addition, effective anti-fouling surfaces, which limit the adhesion of bacteria to a material surface, consist in hydrophilic, highly hydrated, and non-charged surfaces such as those obtained by certain polymer brush coatings and membranes [33].

The survey XPS spectra ranging from 0 to 1200 eV are used to define the elements in different PEO/CNT films deposited by MAPLE. The XPS survey spectra shown in Fig. 2 indicate that carbon and oxygen are the main elements on the surface of the samples and few percent of (Na, S, and Si) as contaminates, most probably from the surfactant in which the CNTs are dispersed. The relative atomic concentration of carbon and oxygen and the ratio of these values are presented in Table 1.

For a detailed analysis of the surface chemistry of samples, high-resolution XPS spectra are recorded in the region of C1s and O1s. The high-resolution carbon (C1s) and oxygen (O1s) XPS spectra are shown in Figs. 3 and 4, respectively. The C1s and O1s overlaid spectra of the as-deposited thin films by MAPLE are shown in Figs. 3a and 4a, respectively. In addition, the O1s and C1s XPS peaks are deconvoluted to better reveal the dispersion of CNTs in the PEO

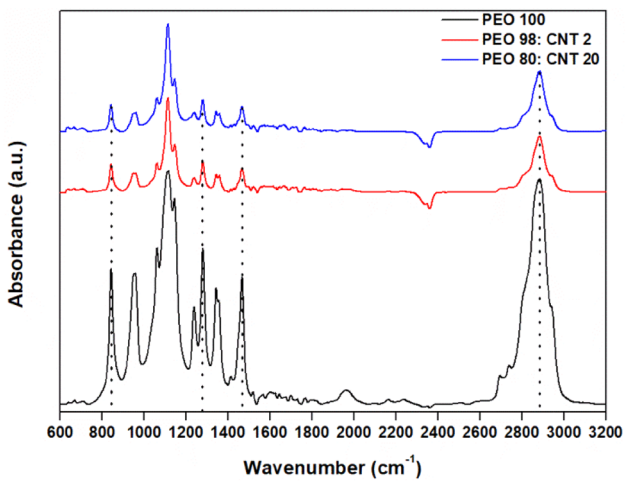

Fig. 1 FTIR spectra of PEO and PEO/CNT films deposited by MAPLE at 750 mJ/cm^2 laser fluence

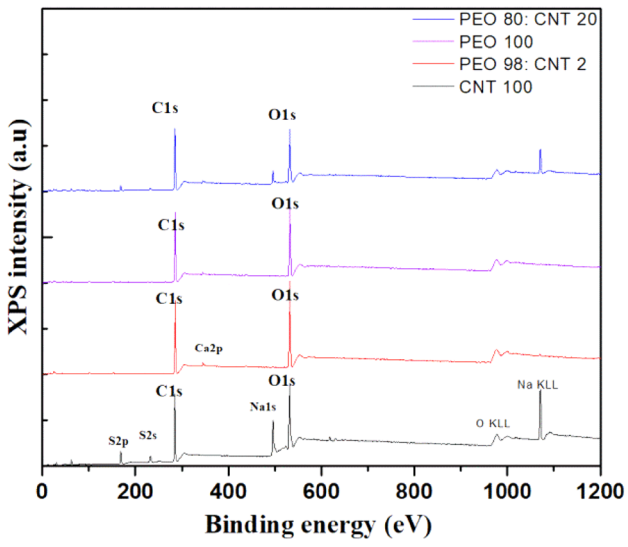

Fig. 2 XPS survey spectra of PEO80:CNT20, PEO100, PEO98:CNT2, and CNT100 films deposited by MAPLE

Table 1 The relative atomic concentration of carbon and oxygen and the ratio of these values

Samples	C1s (%)	O1s (%)	O/C
PEO80:CNT20	74.7	25.3	0.34
PEO100	70.6	29.4	0.42
PEO98:CNT2	66.3	33.7	0.51
CNT100	69.7	30.3	0.43

films. The deconvolution results are shown in Figs. 3b–e and 4b–e, respectively.

The C1 region is fitted considering five components (C1, C2, C3, C4, C5), which are assigned according to the position of carbon binding energy in CNT [34] and PEO [35, 36]. The components are: C=C in sp2 (at 284.6 eV); C–H and C–C in sp3 or defect (at 285.5 eV); C–O and C–C–O single bond (at approximately 286.6 eV); C=O double bonds (at 287.9 eV); and COOH (289.3 eV).

The percentages of each component C1–C5 are plotted together (in Fig. 3f) for comparison. Two types of spectra can be noticed, i.e., where C1-components are predominant and the other two spectra where C3 represent the majority for the samples where PEO are in percent of 98% and 100%.

The as-deposited CNT100 films contain a majority of carbon bonded with other carbon atom in sp2 (C2 of 61%) or carbon single-bonded oxygen (C3 in 26.3%) as shown in Fig. 3f). In the PEO (98% and 100%) samples deposited by MAPLE (Fig. 3c, d), we observe the preservation of main carbon bonding in PEO as C–O–C (C3-ether-type carbon) and the CH_2 (polymer backbone-C2) as reported elsewhere [32] and an additional small percent (~ 1.5%) of ester and carboxylic acid groups that was not present in the other samples.

The XPS spectra recorded in C1s region for the PEO98:CNT2 films deposited by MAPLE nearly match the as-deposited PEO films (see Fig. 3d), while the results obtained for the PEO80:CNT20 films deposited by MAPLE match the as-deposited CNT films (see Fig. 3e). The results obtained indicate that the films with the 20% CNT are CNT-like, while the films with 2% CNT are PEO-like.

The O1s region was fitted considering the usually binding energy at 531.0 eV (O1, double bond O in O=C), at 533 eV (O2 single-bonded O in –O*–C, C–O, HO*–C), and 535.0 eV (O3, attributed to O–COH, COOH). Additional peaks were observed only in the as-deposited CNT and PEO80:CNT20 films, i.e., (Ox) at 532 eV, which can be attributed to chemisorbed oxygen species in CNT and (Ow) at about 536.3 eV (O4 assigned to O in water or O–C–OR). The calculated percentages of these groups (oxygen-containing groups) are plotted in Fig. 4f), where we can see that in the PEO-like samples the highest percentage (89.3% for PEO100 and 92.8%, respectively, for PEO98:CNT2) of oxygen atoms are single bonded to carbon (as we expected in their C–O–C chain), while in the CNT-like sample the majority of oxygen atoms are chemisorbed (60.1% for CNT100 and 47.9 for PEO80:CNT20) with additional water vapors (3.2% and 10%) in between CNT networks.

Thus, the XPS results demonstrate the successful incorporation of CNTs in the PEO polymer thin films via a laser-based approach.

Contact-angle measurements are widely used for the characterization of the hydrophilicity of thin-film surfaces, and the results are presented in Fig. 5. Hydrophilicity is one of the most important properties of thin films, which could influence the anti-fouling ability of the thin films.

The as-deposited PEO100 films have the highest contact angle of 37°, and the contact angle of the CNTs thin films is 11.5°. After incorporation of the hydrophilic low-dimensional carbon nanomaterials, the contact angles of the thin-film blends decreased. For the PEO80:CNT20 films, a minimum contact angle of approx. 19.25° is observed. The reason is that the large amount of hydrophilic groups on the thin-film surface plays a favorable role in increasing the hydrophilicity of the thin-film blend. We can assume that the better hydrophilicity is due to the dispersion of CNTs in the hybrid thin films, making the oxygen-containing functional groups on the thin-film blend surface play their role effectively. As a result, the increased hydrophilicity will play a positive role in promoting thin-film anti-fouling performance. These contact-angle results are in good agreement with the results observed by XPS.

3.2 Morphological investigation

In addition to the surface chemistry, the morphology and topography of a thin-film surface are also important, as previous studies have shown that by tuning the morphology and topography of a surface it is possible to control the formation of biofilms [5]. In [37, 38], it has been reported that by increasing the surface roughness, the bacterial adhesion strength decreases, while other studies have reported the opposite behavior, i.e., smooth surfaces decrease bacterial adhesion [39].

Therefore, in this section, we will investigate the possibility to tune the surface morphology and topography of the laser deposited PEO/CNT films. The surface topography and smoothness of the MAPLE-deposited PEO/CNT coatings deposited on Si(100) substrates were investigated by non-contact AFM. The as-deposited pure PEO and CNT surfaces appear to be rather rough, with a root-mean-square (RMS) roughness of approximately 70 nm. (See Fig. 6.) The AFM image of the CNT film deposited by MAPLE suggests significant aggregation of CNTs on the substrate (similar to what has been reported previously in [16]). In contrast, the RMS roughness decreased for the

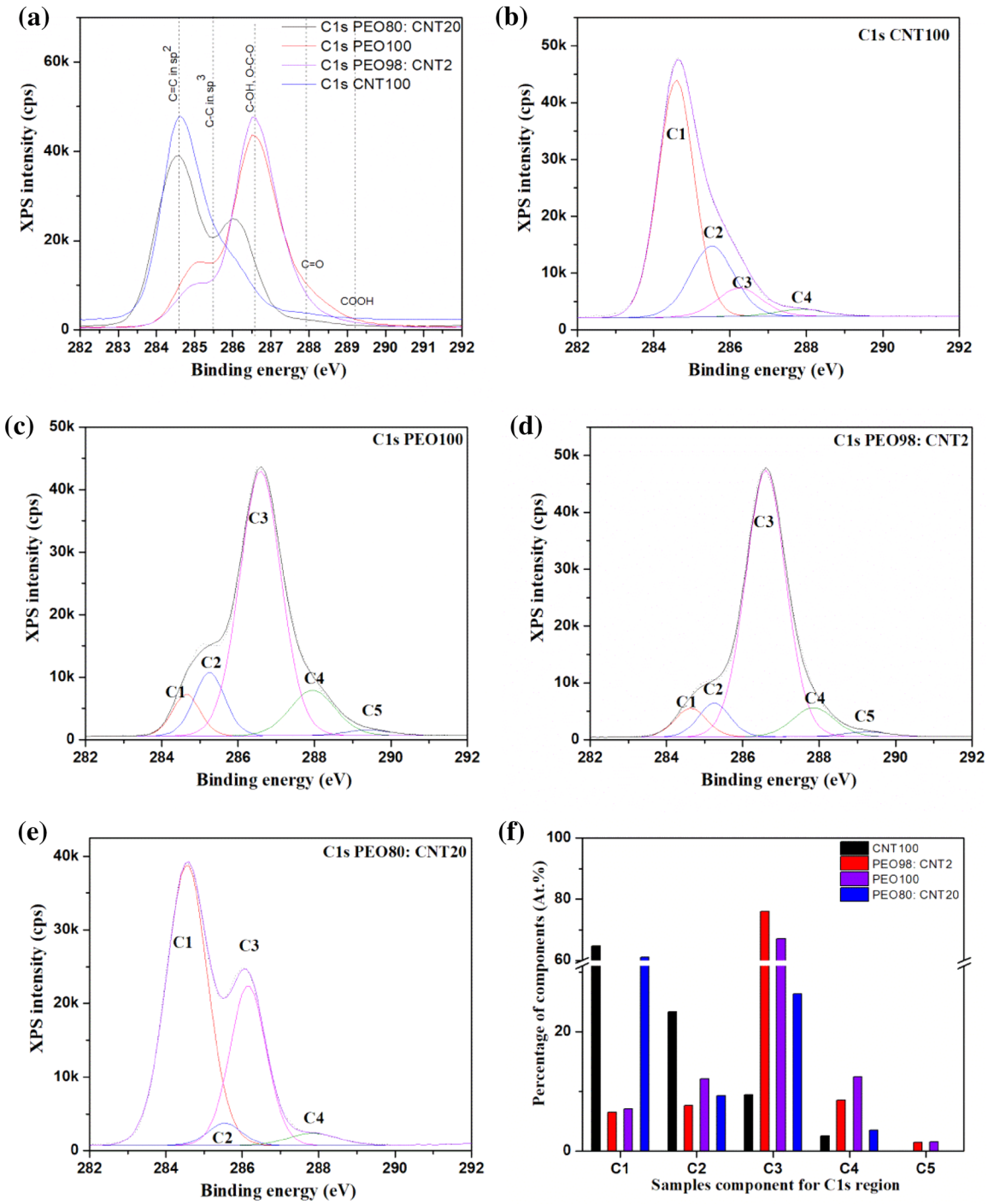

Fig. 3 **a** XPS of the C1s region for CNT, PEO, and PEO/CNT films deposited by MAPLE, and the corresponding fitted deconvolution of the C1s peak for **b** CNT, **c** PEO100, **d** PEO98:CNT2, and **e** PEO80:CNT20; **f** atomic percentage of each component in the carbon region C1–C5

PEO/CNT blends by increasing the CNT content in the sample, i.e., for 2% CNT, the RMS roughness is 24, while for 20% CNT the value of the RMS is around 1 nm. The surfaces of the PEO/CNT blends appear to be uniform, smooth, and featureless, the CNT most probably filling the asymmetries on the PEO films, carpeting the surface completely. Consequently, the CNTs appear to smoothen the surface topography, which is an important finding taking into account the previous work of Wei et al. [40] where it is shown that smooth surfaces inhibit the adhesion of Gram-positive and Gram-negative bacteria.

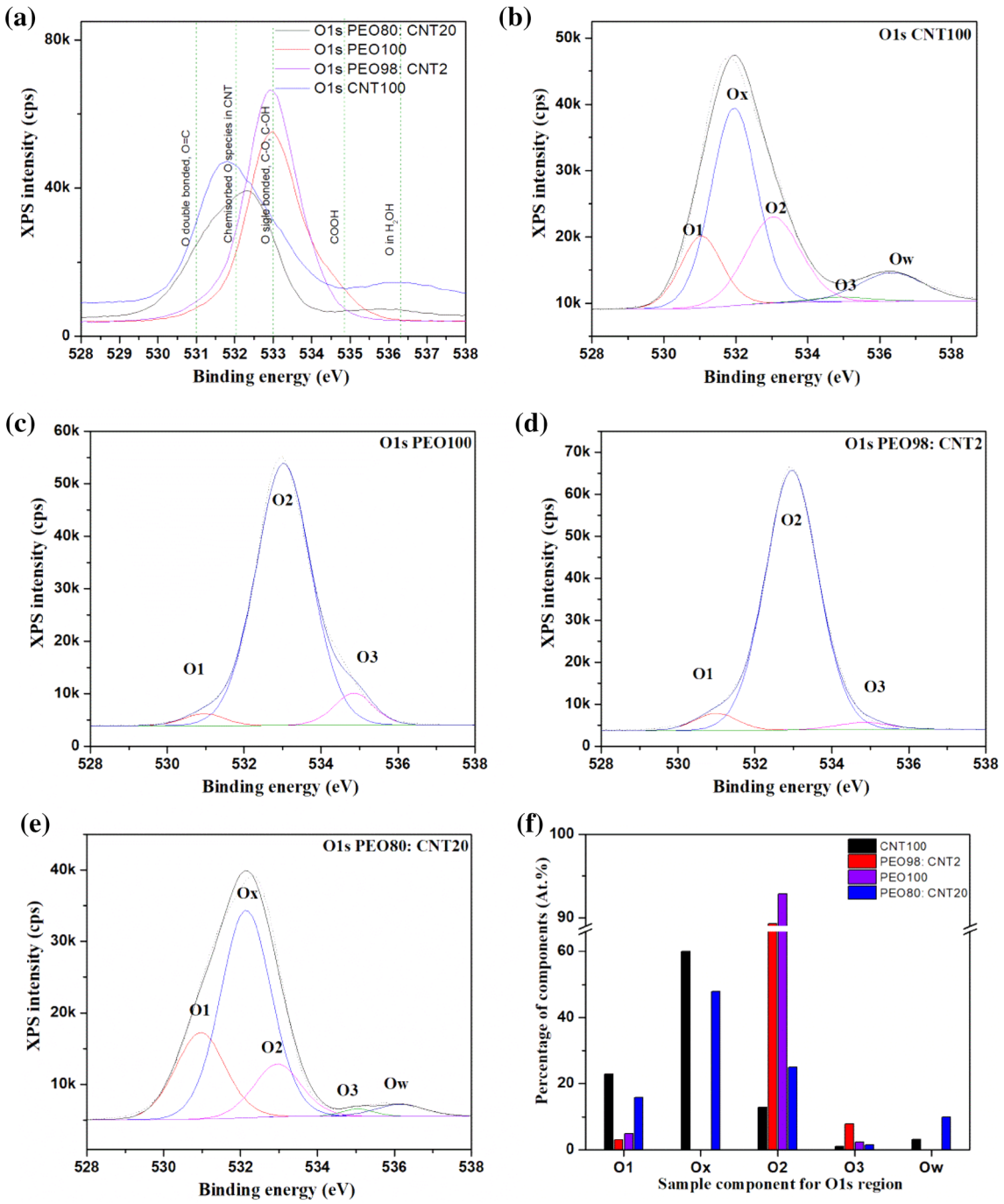

Fig. 4 **a** XPS of the O1s region for CNT, PEO, and PEO/CNT films deposited by MAPLE, and the corresponding fitted deconvolution of the O1s peak for the **b** CNT, **c** PEO100, **d** PEO98:CNT2, and **e** PEO80:CNT20; **f** atomic percentage of each component in the oxygen region

The surface of the PP and PE hernia repair meshes coated with PEO polymer, carbon nanotubes, and polymer/carbon nanotubes has been investigated by scanning electron microscopy and the images are shown in Fig. 7. Similar morphologies have been observed for both types of substrates, i.e., the PP and PE meshes. The morphologies of the as-deposited PEO coatings on the hernia repair meshes exhibit uniform surfaces, with small spherical shaped droplets on the surface, which is an expected characteristic for semicrystalline polymers such as PEO. In addition, the CNT films on the hernia repair meshes cover entirely the hernia repair supports and nanotube bundles (see Fig. 7e), reaching hundreds of nanometers in size

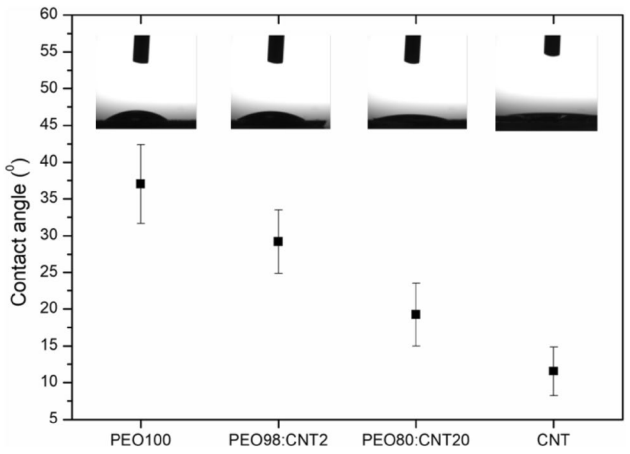

Fig. 5 Water contact angle and the photographs of water drops of the PEO100, PEO98:CNT2, PEO80:CNT20, and CNT100 thin films deposited by MAPLE

which can be noticed (Fig. 7e). These observations are consistent with previous reports by Gyorgy et al. [17].

The texture of the polymer/CNT, i.e., PEO98:CNT2 and PEO80:CNT20 coating surface is roughly the same. The polymer/CNT coatings are continuous, compact, and individually distributed CNTs cannot be distinguished on the surface of the coatings. However, the XPS results shown previously reveal that the CNTs are incorporated in the PEO polymer film. Furthermore, previous molecular dynamic simulation studies [41] have revealed that polymer film formation is the result of an explosive process in which the polymer molecules are ejected as part of matrix–polymer droplets [41, 42]. This is consistent with our observations, as the dominant features which can be observed are nano- and micro-droplets (largest dimension of approximately 10 μm). Corroborating these observations with the AFM results, we may speculate that the low surface roughness of the PEO80:CNT20 films could be attributed to the impact of the target (polymer and carbon nanotubes) molecules with the substrate, i.e., the polymer wets and fills the voids in the carbon nanotubes [15]. We are currently verifying this hypothesis in various experiments. In addition, the polymer/CNT films deposited by MAPLE are crack free. It has been shown in previous studies that the addition of as little as 1.5 wt% CNTs improves fracture toughness [43], wear resistance [39], fatigue suppression, and crack bridging [44].

3.3 Optical investigation

In order to gain information on the optical properties of the polymer/carbon nanotube (PEO/CNT) and study the incorporation and dispersion of the CNTs in the thin-film blends deposited by MAPLE, spectroscopic ellipsometry analysis is carried out. However, as spectroscopic ellipsometry is an indirect technique, based on the change in light polarization reflected from a thin film, and it is thus dependent on the roughness of the surface. Therefore, the experimental data obtained for the pure PEO thin films is affected by experimental errors due to the high roughness (> 70 nm) of the PEO layers.

In order to extract the values of the optical constants and fit the experimental data, an optical model is built. The optical model consists in a stack of different materials, each material characterized by its own dielectric function (optical constants). Due to the fact that the PEO98:CNT2 layer is deposited on silicon, in the optical model constructed, the silicon substrate (with a thickness of 1 mm) is considered the first layer, followed by a very thin native oxide layer (~ 3 nm). The third layer is the PEO98:CNT2 mixture, and the last layer is the rough top layer. In case of the silicon and native oxide substrates, the values of the optical constants are taken from the literature [45]. The top rough layer is estimated to 50% air and 50% PEO/CNT in the Bruggeman approximation [46]. The PEO98:CNT2 layer is composed of carbon graphite and PEO polymer in the effective medium approximation (EMA). The optical constants of the PEO polymer layer are approximated by using a single Gauss oscillator, and the optical constants of carbon are taken from the ellipsometer database [47].

In our optical model, the unknown parameters are: the thickness of the thin films, the thickness of the top rough layer, the optical constants of PEO, the optical constants of the PEO/CNT mixture, and the percent of CNT in this mixture. In order to reduce the number of unknown parameters, the fitting procedure is carried out in a few successive steps. First, the thicknesses of all the layers are approximated by fitting the experimental data with a Cauchy dispersion formula with Urbach tail in the 800–1000 nm wavelength range, where the film is supposed to be optically transparent or to have a small absorption. Thus, the thickness values of the PEO/CNT layer are 254 nm and 5.6 nm for the top rough layers.

In the second step, the values of the thickness are fixed, and the experimental data are fitted on the entire wavelength range (350–1000 nm) by using the mixture of materials in EMA approximation. For the PEO layer, a single Gauss oscillator is used. The Gauss parameters and the percent of CNTs are varied until a minimum value of the mean square error (MSE) is obtained, i.e., the smaller the values of MSE the better the fit [46]. For the smallest value of the MSE, voids are introduced in our EMA model. The composition of the EMA layers obtained is: 4.5% CNT, 21.9% voids, and 73.6% PEO. By using a single Gauss oscillator, the values of the refractive index are $n = 1.43–1.45$ for the pure PEO layer, i.e., a normal value

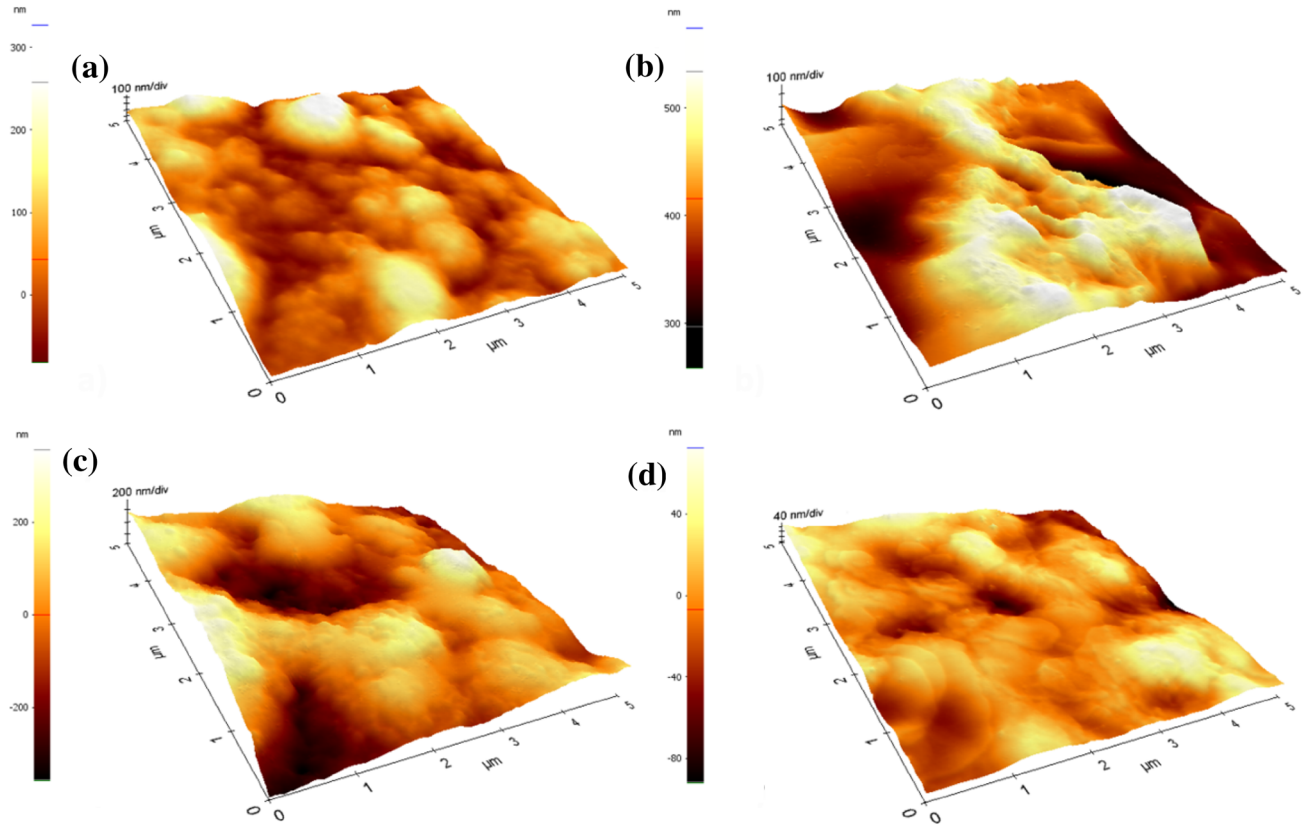

(e)

AFM statistics	PEO 100%	CNT 100%	PEO 80% CNT 20%	PEO 98% CNT 2%
RMS (nm)	69	60	1.3	24
S_P (nm)	32	574	0.35	72
S_v (nm)	-82	258	-0.3	-91

RMS=root mean square, S_p=peak height, S_v= valley height

Fig. 6 AFM images on 5×5 μm^2 areas of **a** PEO 100, **b** CNT 100, **c** PEO 98:CNT 2, and **d** PEO 80:CNT 20 polymer blends deposited by MAPLE onto Si(100) substrates; e) statistical parameters, i.e., root-mean-square (RMS), S_p (peak height), and S_v (valley height) corresponding to each of the AFM images shown in **a**–**d**

for soft materials such as polymers. Once the preliminary values of the optical constants are obtained, we readjusted the thickness values from 254 to 262 nm for PEO98:CNT2 layer.

For the true values of "*n*" and "*k*" for the PEO/CNT, void layers are obtained by fitting point by point the experimental data. The results of this procedure are presented in Fig. 8. The values of the extinction coefficient or of the optical absorption coefficient ($\alpha = 4\pi k/\lambda$) present some large peaks on the measured spectra. The first peak occurs at $\lambda = 380$–400 nm, the second at $\lambda = 580$–650 nm and the third at $\lambda = 980$–1000 nm. Our results are in agreement with the results reported in [48] by Chernysheva et al., where the peaks in the absorption spectrum of CNT obtained by PLD are located 700 nm and 1000 nm.

For comparison, we analyzed the as-deposited CNT thin film in a similar manner to the PEO/CNT film deposited on silicon substrate. The fitting routine is the same as in the case of the blend. First, the thickness of the CNT is approximated by Cauchy–Urbach in the 800–1000 nm wavelength range. Second, the entire measured spectrum is fitted by point-by-point procedure. In this way, we obtain the dispersion of

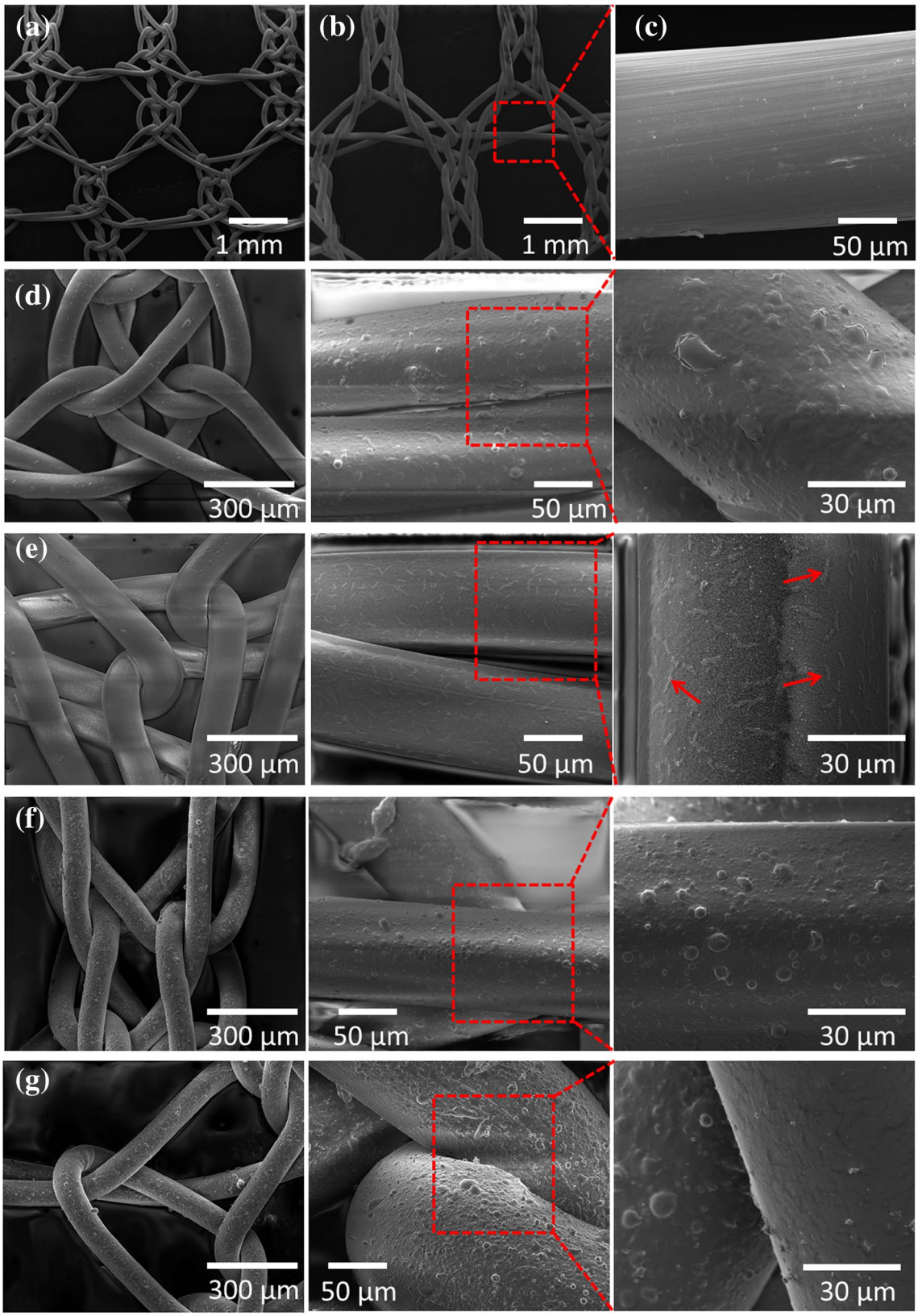
(a)
1 mm
(b)
1 mm
(c)
50 µm
(d)
300 µm
50 µm
30 µm
(e)
300 µm
50 µm
30 µm
(f)
300 µm
50 µm
30 µm
(g)
300 µm
50 µm
30 µm

◂**Fig. 7** SEM images of commercially available **a** polypropylene (PP) and **b** polyester (PE) monofilament, macroporous hernia repair meshes prior to applying the coatings by MAPLE. **c** The red square in **b** marks the magnified SEM image (image on the right) of a single fiber in a polyester hernia repair mesh prior to its deposition by MAPLE. SEM images of PP hernia repair meshes coated with: **d** a PEO film by MAPLE (the image in the middle and on the right are high-magnification SEM images of the PEO film deposited onto a single-mesh fiber); **e** a CNT film by MAPLE (the image in the middle and on the right are high-magnification SEM images of the CNT film deposited onto a single-mesh fiber); the arrows indicate CNT bundles; **f** a PEO98:CNT2 film by MAPLE (the image in the middle and on the right are high-magnification SEM images of the PEO98:CNT2 film deposited onto a single-mesh fiber); and **g** a PEO80:CNT20 film by MAPLE (the image in the middle and on the right are high-magnification SEM images of the PEO80:CNT20 film deposited onto a single-mesh fiber)

optical constants for our CNT thin film, and the result is presented in Fig. 8.

In terms of the extinction coefficient, there are few large peaks: at $\lambda = 650$ nm, $\lambda = 770$ nm, and $\lambda = 900$–970 nm. According to [49], those peaks correspond to exfoliated CNT. In case of PEO98:CNT2 mixture, the peaks located at 770 nm disappears and the other CNT peaks are shifted. A similar result has been reported in [50] where a percentage of 2–4% of carbon nanotubes in a polymer matrix, i.e., poly(3-hexylthiophene-2,5-diyl), leads to an increase in the optical absorption in different optical domains (below 2 eV or above 620 nm–1.2 eV for 2% carbon).

4 Conclusions

In this work, matrix-assisted pulsed laser evaporation technique was optimized for the fabrication of thin films aiming at coating commercial hernia repair meshes. The coatings were produced by depositing polyethylene oxide (PEO) polymer, carbon nanotubes (CNT), and PEO/CNT blends (different experiments) on hernia repair meshes. Our approach is simple and flexible due to the fact that PEO, CNT, and PEO/CNT blends can be easily deposited by MAPLE on various supports, including flat and non-conformal plastics. The proposed deposition route is also efficient due to the fact that PEO, CNT, and PEO/CNT blends are deposited onto the surface by a direct laser deposition method without the need of prior surface functionalization. Surface characterization of the resulting films using infrared spectroscopy (FTIR), X-ray photoelectron spectroscopy (XPS), atomic force microscopy (AFM), and scanning electron microscopy (SEM) corroborated that PEO and PEO/CNT was deposited without any chemical alteration on the surface of the hernia repair meshes. The PEO films became smoother with the addition of CNT. Hence, CNT addition modifies the resulting surface topology and chemistry rendering surfaces coated with our protective layers.

Here we could show for the first time the deposition of polymer/carbon nanotube blends as thin-film coatings onto flexible, non-planar substrates. As the antimicrobial properties of the CNTs have received great attention in the last years, we intend to expand our studies to investigate the antimicrobial effect of the polymer/carbon nanotube coatings fabricated by MAPLE. In addition, it will be interesting to determine the minimum quantity of carbon nanotubes in the polymer/CNT blends which renders the highest antimicrobial effect toward different bacteria. We believe that this study, i.e., the demonstration of hybrid coatings with controllable morphology and chemistry by laser-based methods might represent a solution for potential application in standard hernia repair.

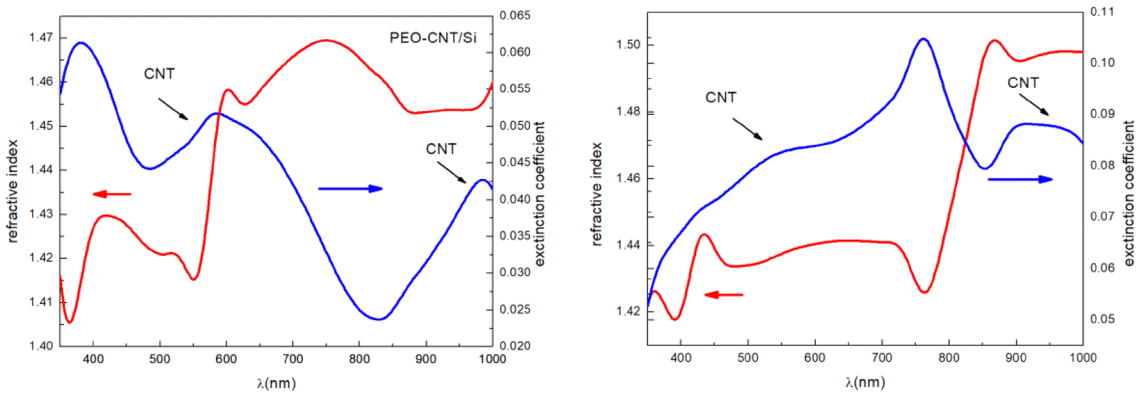

Fig. 8 The refractive index and extinction coefficient spectra for the PEO98:CNT2 thin film (left) and for the CNT100 thin film (right), obtained by point-by-point fit

Acknowledgements Financial support from NILPRP, through the LAPLAS VI NUCLEU program no. 16N/08.02.2019, and UEFISCDI, through the PED project no. PN-III-P2-2.1-PED-2016-1715 (HERMESH) is gratefully acknowledged. The authors would like to thank Dr. Andreea Matei for acquiring the XPS spectra and Valentina Mărăscu for acquiring the FTIR spectra.

References

1. K. Baylón, P. Rodríguez-Camarillo, A. Elías-Zúñiga, J.A. Díaz-Elizondo, R. Gilkerson, K. Lozano, Past, present and future of surgical meshes: a review. Membranes **7**, 47 (2017)
2. S. Elango, S. Perumalsamy, K.R.B. Tech, K. Vadodaria, Mesh materials and hernia repair. BioMedicine **7**(3), 14 (2017)
3. P.T. Hammond, Building biomedical materials layer-by-layer. Mater. Today **15**(5), 196 (2012)
4. K. Hori, S. Matsumoto, Bacterial adhesion: from mechanism to control. Biochem. Eng. J. **48**, 424 (2010)
5. D. Campoccia, L. Montanaro, C.R. Arciola, A review of the biomaterials technologies for infection-resistant surfaces. Biomaterials **34**, 8534 (2013)
6. Y. Bilsel, I. Abci, The search for ideal hernia repair; mesh materials and types. Int. J. Surg. **10**, 317 (2012)
7. F. Siedenbiedel, J.C. Tiller, Antimicrobial polymers in solution and on surfaces: overview and functional principles. Polymers **4**, 46 (2012)
8. F. Fuertges, A. Abuchowski, The clinical efficacy of poly(ethylene glycol)-modified proteins. J. Control. Release **11**, 139 (1990)
9. P.K. Working et al., Safety of poly(ethylene glycol) and poly(ethylene glycol) derivatives, in *Polyethylene Glycol Chemistry and Biological Applications*, ed. by J.M. Harris, S. Zalipsky (American Chemical Society, Washington DC, 1997), p. 45
10. R.I. Mahato, Biomaterials for delivery and targeting of proteins and nucleic acids. CRC Press Ald. Cat. No. Z705102 (2005)
11. S. Kang, M. Pinault, L.D. Pfefferle, M. Elimelech, Single-walled carbon nanotubes exhibit strong antimicrobial activity. Langmuir **23**, 8670 (2007)
12. S. Aslan, C. Zoican Loebick, S. Kang, M. Elimelech, L.D. Pfefferle, P.R. Van Tassel, Antimicrobial biomaterials based on carbon nanotubes dispersed in poly(lactic-co-glycolic acid). Nanoscale **2**, 1789 (2010)
13. D.B. Chrisey, A. Piqué, R.A. McGill, J.S. Horwitz, B.R. Ringeisen, D.M. Bubb, P.K. Wu, Laser deposition of polymer and biomaterial films. Chem. Rev. **103**(2), 553 (2003)
14. J. Schou, Physical aspects of the pulsed laser deposition technique: the stoichiometric transfer of material from target to film. Appl. Surf. Sci. **255**, 5191 (2009)
15. P.K. Wu, J. Fitzgerald, A. Pique, D.B. Chrisey, R.A. McGill, Deposition of nanotubes and nanotube composites using matrix-assisted pulsed laser evaporation. Mater. Res. Soc. Symp. Proc. **617**, J2.3.1-6 (2000)
16. A. Perez del Pino, E. Gyorgy, L. Cabana, B. Ballestros, G. Tobias, Deposition of functionalized single wall carbon nanotubes through matrix assisted pulsed laser evaporation. Carbon **50**, 4450 (2012)
17. E. Gyorgy, A. Perez del Pino, J. Roqueta, B. Ballestros, L. Cabana, G. Tobias, Effect of laser radiation on multi-wall carbon nanotubes: study of shell structure and immobilization process. J. Nanopart. Res. **15**, 1852 (2013)
18. I.A. Paun, A.M. Acasandrei, C.R. Luculescu, C.C. Mustaciosu, V. Ion, M. Mihailescu, E. Vasile, M. Dinescu, MAPLE deposition of polypyrrole-based composite layers for bone regeneration. Appl. Surf. Sci. **357**, 975–984 (2015)
19. R. Cristescu, A. Doraiswamy, T. Patz, G. Socol, S. Grigorescu, E. Axente, F. Sima, R.J. Narayan, D. Mihaiescu, A. Moldovan, I. Stamatin, I.N. Mihailescu, B. Chisholm, D.B. Chrisey, Matrix assisted pulsed laser evaporation of poly(D, L-lactide) thin films for controlled-release drug systems. Appl. Surf. Sci. **253**, 7702 (2007)
20. I.A. Paun, V. Ion, A. Moldovan, M. Dinescu, Thin films of polymer blends for controlled drug delivery deposited by matrix-assisted pulsed laser evaporation. Appl. Phys. Lett. **96**, 243702 (2010)
21. C. Constantinescu, A. Palla-Papavlu, A. Rotaru, P. Florian, F. Chelu, M. Icriverzi, A. Nedelcea, V. Dinca, A. Roseanu, M. Dinescu, Multifunctional thin films of lactoferrin for biochemical use deposited by MAPLE technique. Appl. Surf. Sci. **255**, 5491 (2009)
22. R. Rella, J. Spadavecchia, M.G. Manera, S. Capone, A. Taurino, M. Martino, A.P. Caricato, T. Tunno, Acetone and ethanol solid-state gas sensors based on TiO_2 nanoparticles thin film deposited by matrix assisted pulsed laser evaporation. Sens. Actuators B **127**, 426 (2007)
23. A.P. Caricato, A. Luches, R. Rella, Nanoparticle thin films for gas sensors prepared by matrix assisted pulsed laser evaporation. Sensors **9**(4), 2682 (2009)
24. A.T. Sellinger, E.M. Leveugle, K. Gogick, L.V. Zhigilei, J.M. Fitz-Gerald, Laser processing of polymer nanocomposite thin films. J. Vacuum Sci. Technol. A **24**, 1618 (2006)
25. H. Jeong, S. Napolitano, C.B. Arnold, R.D. Priestley, Irreversible adsorption controls crystallization in vapour-deposited polymer thin films. Phys. Chem. Lett. **8**, 229–234 (2017)
26. H. Jeong, K.S. Shepard, G.E. Purdum, Y. Guo, Y.-L. Loo, C.B. Arnold, R.D. Priestley, Additive growth and crystallization of polymer films. Macromolecules **49**, 2860–2867 (2016)
27. Y. Wang, H. Jeong, M. Chowdhury, C.B. Arnold, R.D. Priestley, Exploiting physical vapour deposition for morphological control in semi-crystalline polymer films. Polym. Crystal. **1**, e10021 (2018)
28. D.M. Bubb, J.S. Horwitz, R.A. McGill, D.B. Chrisey, M.R. Papantonakis, R.F. Haglund Jr., B. Toftmann, Resonant infrared pulsed-laser deposition of a sorbent chemoselective polymer. Appl. Phys. Lett. **79**, 17 (2001)
29. A. Palla-Papavlu, V. Dinca, M. Dinescu, F. Di Pietrantonio, D. Cannatà, M. Benetti, E. Verona, Matrix-assisted pulsed laser evaporation of chemoselective polymers. Appl. Phys. A **105**, 651 (2011)
30. E.C. Stancu, A.M. Stanciuc, S. Vizireanu, C. Luculescu, L. Moldovan, A. Achour, G. Dinescu, Plasma functionalization of carbon nanowalls and its effect on attachment of fibroblast-like cells. J. Phys. D Appl. Phys. **47**(26), 265203 (2014)
31. R.M. Silverstein, G.C. Bassler, *Spectrometric Identification of Organic Compounds* (Wiley, New York, 1964)
32. V. Tucureanu, A. Matei, A.M. Avram, FTIR spectroscopy for carbon family study. Crit. Rev. Anal. Chem. **46**(6), 502–520 (2016)
33. W.-Y. Wang, J.-Y. Shi, J.-L. Wang, Y.-L. Li, N.-N. Gao, Z.-X. Liu, W.-T. Lian, Preparation and characterization of PEG-*g*-MWCNTs/PSf nano-hybrid membranes with hydrophilicity and anti-fouling properties. RSC Adv. **5**, 84746–84753 (2015)
34. C.M. Damian, A.M. Pandele, C. Andronescu, A. Ghebaur, S.A. Garea, H. Iovu, Epoxy-based nanocomposites reinforced with new amino functionalized multi-walled carbon nanotubes. Fullerenes Nanotubes Carbon Nanostruct. **19**, 197–209 (2011)
35. D. Briggs, D.M. Brewis, R.H. Dahm, I.W. Fletcher, Analysis of the surface chemistry of oxidized polyethylene: comparison of XPS and ToF-SIMS. Surf. Interface Anal. **35**, 156–167 (2003)
36. M.A. Cole, H. Thissen, D. Losic, N.H. Voelcker, A new approach to the immobilisation of poly(ethylene oxide) for the reduction of

non-specific protein adsorption on conductive substrates. Surf. Sci. **601**(7), 1716–1725 (2007)
37. N. Mitik-Dineva, J. Wang, V.K. Truong, P. Stoddart, F. Malherbe, R.J. Crawford, E.P. Ivanova, *Escherichia coli*, *Pseudomonas aeruginosa*, and *Staphylococcus aureus* attachment patterns on glass surfaces with nanoscale roughness. Curr. Microbiol. **58**(3), 268–273 (2009)
38. N. Mitik-Dineva, J. Wang, R.C. Mocanasu, P.R. Stoddart, R.J. Crawford, E.P. Ivanova, Impact of nano-topography on bacterial attachment. Biotechnol. J. **3**, 536–544 (2008)
39. C.R. Arciola, M.C. Maltarello, E. Cenni, A. Pizzoferrato, Disposable contact lenses and bacterial adhesion. In vitro comparison between ionic/high-water-content and non-ionic/low-water-content lenses. Biomoterials **16**, 685–690 (1995)
40. L. Wei, J. Luo, Y. Deng, Y. Sun, Biomaterials immobilized with chitosan for rechargeable antimicrobial drug delivery. J. Biomed. Mater. Res. Part A **101**(2), 447–455 (2013)
41. E. Leveugle, L.V. Zhigilei, Molecular dynamics simulation study of the ejection and transport of polymer molecules in matrix-assisted pulsed laser evaporation. J. Appl. Phys. **102**, 074914 (2007)
42. A.P. Caricato, W. Ge, A.D. Stiff-Roberts, Chapter 10: UV- and RIR-MAPLE: fundamentals and applications, in *Advances in the Application of Lasers in Materials Science, Springer Series in Materials Science*, vol. 274, ed. by P.M. Ossi (Springer, Berlin, 2018), pp. 275–308
43. A.K. Keshri, J. Huang, V. Singh, W. Choi, S. Seal, A. Agarwal, Synthesis of aluminum oxide coating with carbon nanotube reinforcement produced by chemical vapor deposition for improved fracture and wear resistance. Carbon **48**, 431–442 (2010)
44. W. Zhang, R.C. Picu, N. Koratkar, The effect of carbon nanotube dimensions and dispersion on the fatigue behavior of epoxy nanocomposites. Nanotechnology **19**, 5 (2008)
45. C.M. Herzinger, B. Johs, W.A. McGahan, J.A. Woollam, W. Paulson, Ellipsometric determination of optical constants for silicon and thermally grown silicon dioxide via a multi-sample, multi-wavelength, multi-angle investigation. J. Appl. Phys. **83**, 6 (1998)
46. H. Fujiwara, *Spectroscopic Ellipsometry Principles and Applications* (Maruzen Co., Ltd., Tokyo, 2007). ISBN 978-0-470-01608-4
47. A. Borghesi, G. Guizzetti, in *Handbook of Optical Constants of Solids II*, ed. by E.D. Palik (Academic, Boston, 1991), pp. 449–460
48. M. Chernysheva, A. Rozhin, Y. Fedotov, C. Mou, R. Arif, S.M. Kobtsev, E.M. Dianov, S.K. Turitsyn, Carbon nanotubes for ultrafast fibre lasers. Nanophotonics **6**(1), 1–30 (2017)
49. https://www.sigmaaldrich.com/catalog/product/aldrich/704148?lang=en®ion=RO. Product no. 704148
50. E. Lioudakis, C. Kanari, A. Othonos, I. Alexandrou, Direct observation of excitons in polymer/carbon nanotube composites at room temperature: the influence of nanotube concentration. Diam. Relat. Mater. **17**, 1600–1603 (2008)